Transverse stability in a Stark decelerator

Sebastiaan Y. T. van de Meerakker,[1,2] Nicolas Vanhaecke,[1] Hendrick L. Bethlem,[1,2] and Gerard Meijer[1]
[1]*Fritz-Haber-Institut der Max-Planck-Gesellschaft, Faradayweg 4-6, 14195 Berlin, Germany*
[2]*FOM-Institute for Plasmaphysics Rijnhuizen, Edisonbaan 14, 3439 MN Nieuwegein, The Netherlands*
(Received 28 April 2005; revised manuscript received 8 November 2005; published 1 February 2006)

The concept of phase stability in a Stark decelerator ensures that polar molecules can be accelerated, guided, or decelerated without loss; molecules within a certain position and velocity interval are kept together throughout the deceleration process. In this paper the influence of the transverse motion on phase stability in a Stark decelerator is investigated. For typical deceleration experiments—i.e., for high values of the phase angle ϕ_0—the transverse motion considerably enhances the region in phase space for which phase stable deceleration occurs. For low values of ϕ_0, however, the transverse motion reduces the acceptance of a Stark decelerator and unstable regions in phase space appear. These effects are quantitatively explained in terms of a coupling between the longitudinal and transverse motion. The predicted longitudinal acceptance of a Stark decelerator is verified by measurements on a beam of OH ($X\,^2\Pi_{3/2}, J=3/2$) radicals passing through a Stark decelerator.

DOI: 10.1103/PhysRevA.73.023401 PACS number(s): 33.80.Ps, 33.55.Be, 39.10.+j

I. INTRODUCTION

In recent years our group has developed the so-called Stark deceleration technique. In this technique, the interaction of polar molecules in a molecular beam with inhomogeneous time-varying electric fields is exploited to change the longitudinal velocity of the molecules. Using arrays of electric field stages that are switched to high voltage at the appropriate times, a part of the molecular beam is selected and can be transferred to any arbitrary velocity. Bunches of state-selected molecules are produced with a computer-controlled velocity and with a low longitudinal temperature [1]. The Stark decelerator for neutral polar molecules is the equivalent of a linear accelerator (LINAC) for charged particles. By now, molecular beam decelerators have successfully been implemented by other groups as well [2,3]; in several other laboratories, a Stark decelerator is planned or under construction.

The Stark decelerator is a convenient and versatile tool to produce slow molecular beams and is of particular relevance to the field of cold molecules [4,5]. When the Stark decelerator is extended with a trap, molecules can be decelerated to rest and confined in the trap for times up to seconds. Using this approach, trapping of ND_3 molecules [6,7] and OH radicals [8] has been demonstrated to date, offering new and interesting possibilities to study interactions of polar molecules in the mK range. Alternatively, after deceleration to about 100 m/s, the molecules can be injected and confined in an electrostatic storage ring [9]. Other applications of Stark decelerated (and/or trapped) molecules include high-resolution spectroscopy [10], the accurate determination of quantum-state specific lifetimes of molecules [11], and molecular beam scattering experiments.

In analogy to the operation of a LINAC [12], the concept of phase stability is essential for the operation of a Stark decelerator [13,14]. Phase stability governs the motion of the molecules through the Stark decelerator and ensures that the velocity of the selected part of the beam can be varied without loss; molecules within a certain position and velocity interval are kept together throughout the deceleration process independent of the length of the decelerator. The molecular beam is thus decelerated, maintaining the high phase-space density that is present in a pulsed molecular beam; phase stability guarantees that the shape of the phase-space distribution of the decelerated package of molecules can be equal at the exit and entrance of the Stark decelerator. The same concept of phase stability applies to optical analogs of the Stark decelerator [15,16]. For the electric field deceleration of atoms and molecules in Rydberg states [17,18], schemes that employ phase stability have also been brought forward [19].

The first description and experimental demonstration of phase stability in a Stark decelerator was given by Bethlem *et al.* [13] using a beam of metastable CO molecules. The developed model for phase stability accurately describes the longitudinal motion of molecules in a Stark decelerator and predicts the longitudinal acceptance of the decelerator. Recently, we presented an extended model for longitudinal phase stability, including higher-order terms in the analysis [20]. The extended model predicts a variety of additional phase stable regions, referred to as resonances, whose existence has been experimentally verified.

In the model for longitudinal phase stability, the motion of molecules through a Stark decelerator is treated one dimensionally; i.e., the trajectories of the molecules are assumed to be along the molecular beam axis. In a laboratory Stark decelerator, however, the molecular beam also has a velocity component perpendicular to the molecular beam axis. The electric field geometry in the decelerator drives the selected molecules back towards the molecular beam axis, resulting in a transverse oscillatory motion. One may wonder if and how this transverse motion effects the longitudinal motion of the molecules. In this paper, the influence of the transverse motion on phase stability in a Stark decelerator is studied. Numerical simulations indicate that for high values of the phase angle ϕ_0 the acceptance of a Stark decelerator is significantly larger than the one-dimensional model predicts. For low values of ϕ_0, however, the transverse motion reduces the acceptance and unstable regions in phase space appear. These effects are quantitatively explained in terms of

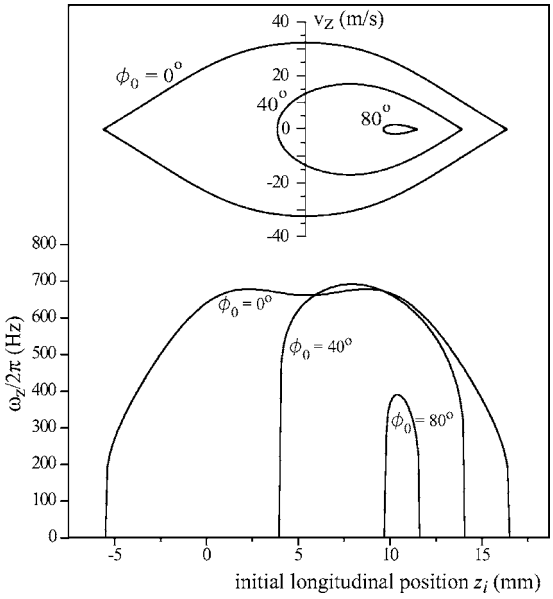

FIG. 1. The natural longitudinal frequencies $\omega_z/2\pi$ for an OH radical in the $M_J\Omega=-9/4$ component of the $X^2\Pi_{3/2}$, $v=0$, $J=3/2$ rotational ground state for the phase angles $\phi_0=0°$, 40°, and 80° as a function of the initial longitudinal position z_i. For these phase angles, the longitudinal phase-space acceptance diagrams that follow from the 1D model for phase stability are shown in the upper part.

a coupling between the transverse and longitudinal motion. The predicted deviation of the longitudinal acceptance of a Stark decelerator from the acceptance that follows from the one-dimensional model is verified by measurements on a beam of OH ($X\,^2\Pi_{3/2}, J=3/2$) radicals passing through a Stark decelerator.

II. LONGITUDINAL PHASE STABILITY

The main results of the one-dimensional model for longitudinal phase stability in a Stark decelerator can be found in Refs. [13,14,20–22]. In the description for phase stability the synchronous molecule and the phase angle ϕ_0 play an essential role. The synchronous molecule is the molecule that is always in phase with the fields that are being switched; i.e., the synchronous molecule loses a constant amount of kinetic energy per stage. The phase angle ϕ_0 at which the decelerator is operated determines both the deceleration rate and the longitudinal acceptance of the decelerator. For a given value of ϕ_0, molecules that have a position in phase space that is within the acceptance of the decelerator, bound by the separatrix, are phase stable and are selected by the decelerator. The separatrices for an OH radical in the $M_J\Omega=-9/4$ component of the $X\,^2\Pi_{3/2}$, $v=0$, $J=3/2$ rotational ground state for the phase angles $\phi_0=0°$, 40°, and 80° are given in the upper part of Fig. 1. Molecules that are within this region will rotate in longitudinal phase space around the position of the synchronous molecule. The longitudinal oscillation frequency $\omega_z/2\pi$[1] depends on the initial longitudinal phase-space position of the molecule. In the remainder of this paper the initial longitudinal phase-space position of a molecule is taken along the line with constant velocity, given by the velocity of the synchronous molecule. The position along this line is indicated by z_i, such that the electrodes of adjacent stages are at $z_i=0$ mm and $z_i=11$ mm (the electric field stages of the decelerator are centered a distance $L=11$ mm apart) and such that the synchronous molecule for $\phi_0=0°$ is initially at $z_i=5.5$ mm. Restriction of the initial position to points along this line can be done without loss of generality, as any isoenergy contour within the separatrix crosses this line. The natural longitudinal frequencies are shown in Fig. 1 as a function of z_i, for the phase angles $\phi_0=0°$, 40°, and 80°. The longitudinal oscillation frequency is maximal when the initial longitudinal position of a molecule is close to the position of the synchronous molecule. Further outward, the oscillation frequency is lowered, reaching zero on the separatrix. For OH radicals in the above-mentioned quantum state, the maximum longitudinal frequency is approximately 700 Hz when the Stark decelerator that is used in the experiments in this paper (*vide infra*) is operated at a phase angle $\phi_0=0°$. The slightly reduced frequency around the synchronous molecule when the decelerator is operated at $\phi_0=0°$ is caused by the nonlinear Stark effect of the OH radical for low values of the electric field strength, but simulations indicate that this effect hardly influences the structure of the phase-space distributions discussed in this paper.

In the extended one-dimensional model for phase stability [20] it is demonstrated that multiple synchronous molecules, with different longitudinal velocities, can exist simultaneously if the Stark decelerator is operated at a phase angle $\phi_0=0°$. The existence of a synchronous molecule with the corresponding phase-stable region is referred to as a resonance, labeled by the parameter s.

III. TRANSVERSE STABILITY

A. Transverse motion

In a Stark decelerator, the electric field is maximal close to the surfaces of the opposing electrodes in a field stage. In this paper, the molecular beam axis is along the z direction, while x and y are the transverse coordinates. Consider an electric field stage where the electrodes are oriented along the x direction. Molecules in a low-field seeking state that approach (along the z axis) these electrodes experience a focusing force towards the molecular beam axis in the y direction; the force in the x direction is negligible. The electric field stages in the decelerator are alternatingly positioned in the x and y directions to obtain a focusing force in both transverse directions. As a consequence, molecules that have an off-axis position and/or velocity component will oscillate around the molecular beam axis. This property is as essential

[1]The formula for the longitudinal oscillation frequencies that is given in our recent paper on longitudinal phase stability (Eq. (10) of Ref. [20]) contains an error, and should read $\omega_z/2\pi=\sqrt{na_n\cos n\phi_0/2m\pi sL^2}$.

for the operation of a Stark decelerator as the longitudinal phase stability; the spreading out of the selected part of the molecular beam is prevented in both the transverse and longitudinal directions.

A quantitative analysis of the intrinsic focusing properties of the decelerator can be obtained when the transverse force is calculated that a molecule experiences during its flight through the decelerator. We will follow here the method that has been used before to calculate the average transverse force for the ND_3 molecule in a Stark decelerator [14].[2] The actual transverse force experienced by a molecule depends in general on its position and time. In this paper, we assume that the motions in the x and y directions are uncoupled and can be treated independently. The validity of this approach is confirmed by numerical simulations. The transverse oscillation time is much larger than the time it takes the molecule to traverse one period (two stages) of the decelerator. The transverse motion can therefore be described by introducing the average force components $\bar{F}_{x,y}$, which are obtained by integrating over one period of the decelerator. The average transverse force only depends on the phase angle ϕ. The longitudinal oscillation frequency $\omega_z/2\pi$ is sufficiently low that, to a good approximation, all molecules within the longitudinal acceptance area travel a distance $2L$ in the time interval $2\Delta T$. In the calculation of the average force the transverse position is taken constant in the time interval $2\Delta T$, since the transverse motion is slow. The average force $\bar{F}_y(\phi)$ then reads

$$\bar{F}_y(\phi) = \frac{1}{2\Delta T}\int_t^{t+2\Delta T} F_y(z(t'),t')dt' \approx \frac{1}{2L}\int_{\phi L/\pi}^{(\phi+2\pi)L/\pi} F_y(z)dz. \tag{1}$$

To a good approximation, the transverse force $\bar{F}_y$ is linear in the displacement y from the molecular beam axis. The strength of the transverse force can therefore be expressed in terms of a frequency $\omega_y(\phi)$, referred to as the natural transverse frequency, using the relation

$$\bar{F}_y = -m\omega_y^2(\phi)y. \tag{2}$$

In Fig. 2, the natural transverse oscillation frequency of the Stark decelerator is shown for an OH ($X^2\Pi_{3/2}, J=3/2, M_J\Omega=-9/4$) radical as a function of the phase ϕ. For a molecule at $\phi=0°$, the natural transverse oscillation frequency is minimal and has a value of only 110 Hz. For increasing longitudinal phases, the natural transverse frequency increases quickly, reaching a maximum of about 750 Hz for $\phi=180°$.

The increasing transverse oscillation frequency for increasing values of ϕ can be understood from the longitudinal motion of the molecules. When the Stark decelerator is operated at $\phi_0=0°$, the synchronous molecule will only fly a maximum distance $L/2$ (5.5 mm for the decelerator discussed here) away from the electrodes that are grounded before the fields are being switched. The synchronous molecule is therefore always closer to the set of electrodes that is grounded than to the set that is at high voltage. This implies that the synchronous molecule is always in the region where the transverse focusing force is only modest and the corresponding transverse oscillation frequency is low. Nonsynchronous molecules oscillate in longitudinal phase space around the position of the synchronous molecule and hence come closer to the position of the electrodes that are at high voltage. Molecules with an ever larger displacement in longitudinal phase space from the position of the synchronous molecule will be focused more efficiently and follow a transverse oscillatory motion with a higher oscillation frequency.

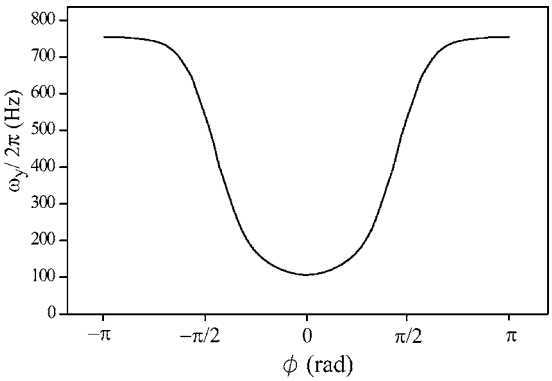

FIG. 2. Natural transverse oscillation frequency $\omega_y/2\pi$ of the Stark decelerator for an OH ($X^2\Pi_{3/2}$, $J=3/2$, $M_J\Omega=-9/4$) radical as a function its phase ϕ.

Generally, a molecule oscillates in phase around the synchronous molecule. The time dependence of the transverse force that a (nonsynchronous) molecule experiences during its flight through the decelerator can be calculated if the phase $\phi(t)$ of the molecule as a function of time that follows from the natural longitudinal frequency $\omega_z/2\pi$ is known. The natural longitudinal and transverse frequencies, presented in Figs. 1 and 2, together in principle govern the complete dynamics of molecules in the Stark decelerator. It is seen from these figures that the longitudinal and transverse oscillation frequencies can become rather similar. One can expect, therefore, that a coupling between the longitudinal and transverse motion can result in parametric amplification, leading to unstable operation of the decelerator. In the next section we present numerical trajectory simulations, to investigate the influence of the transverse motion on the longitudinal acceptance of a Stark decelerator.

B. Longitudinal phase stability: Three dimensions versus one dimension

The effect of the transverse motion of the molecules on the longitudinal acceptance of the decelerator can be studied by comparing the longitudinal acceptance of the Stark decelerator, which is calculated assuming (i) that the molecules fly along the molecular beam axis [referred to as a one-dimensional (1D) calculation] and (ii) taking the real trajectories of the molecules into account (3D calculation). We restrict ourselves here to numerical studies of the trajectories of OH ($X^2\Pi_{3/2}, v=0, J=3/2, M_J\Omega=-9/4$) radicals that pass

[2] In Ref. [14] an error was made when performing the integral [Eq. (5) of Ref. [14]], leading to too high values for the force constants.

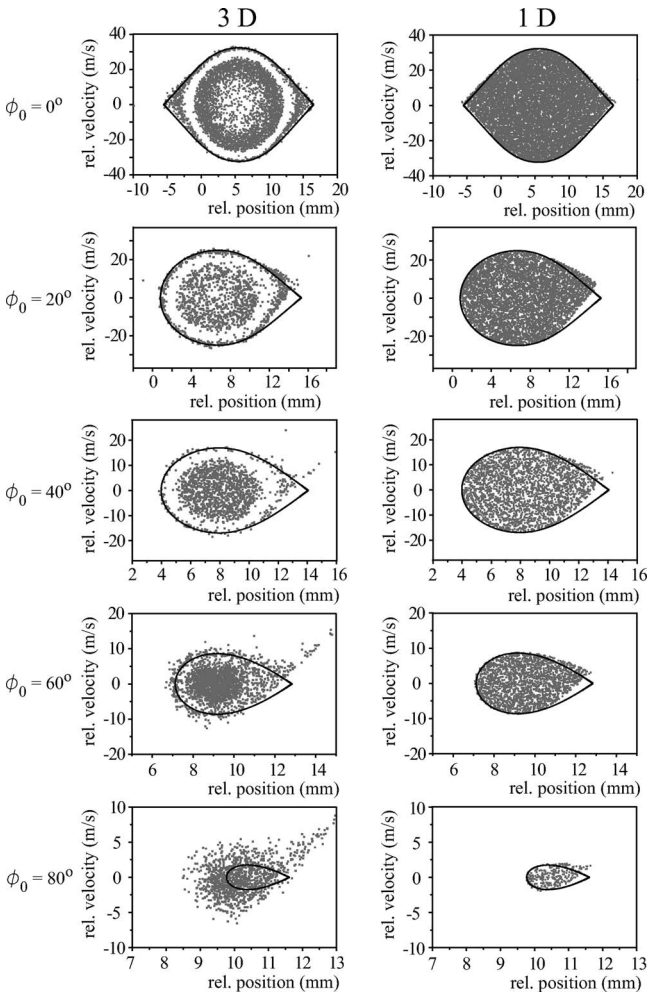

FIG. 3. Longitudinal phase-space distributions of OH ($X^2\Pi_{3/2}$, $J=3/2$, $M_J\Omega=-9/4$) radicals inside the decelerator that result from 1D and 3D trajectory simulations when the Stark decelerator is operated at $\phi_0=0°$, 20°, 40°, 60°, and 80°. In all simulations, the molecules spend approximately 8 ms in the decelerator.

through a Stark decelerator. Furthermore, we limit ourselves in this section to the resonance $s=1$. The influence of the transverse motion on resonances with $s>1$ will be discussed in Sec. III F. In the calculations presented in this paper, a Stark decelerator is simulated that is available in our laboratory (*vide infra*). In the simulations only the length of the decelerator is varied, as will be described below.

A profound difference in the longitudinal acceptance of the decelerator is found for the one- and three-dimensional trajectory calculations. This is illustrated in Fig. 3. For different values of the phase angle ϕ_0, the trajectories of a package of molecules are simulated using a 1D and a 3D trajectory simulation. The resulting longitudinal phase-space distributions of the molecules in the last electric field stage of the decelerator are shown on the left- (3D) and right- (1D) hand sides of Fig. 3. The separatrices that follow from the 1D model for phase stability are given as an overlay. The horizontal and vertical scales for each distribution are different for reasons of clarity. For each value of ϕ_0, the time sequence of the decelerator is chosen such that the total time of flight of the synchronous molecule in the decelerator is approximately 8 ms and the final velocity of the synchronous molecule is about 70 m/s. This is achieved by an appropriate choice of the initial velocity of the synchronous molecule and the length of the decelerator. This strategy allows for a good comparison between the observed phase-space distributions for different values of ϕ_0. For the phase angle $\phi_0=0°$ a velocity of 250 m/s for the synchronous molecule is chosen. In the 1D (3D) simulations, the molecules are homogeneously distributed over a 2D surface (6D volume) in phase space at the entrance of the decelerator that largely exceeds the 2D (6D) acceptance of the decelerator. It is important to note that the phase-space densities (number of molecules that are used in the simulation per unit area/volume) in each of the simulations is different to limit the computational time. Therefore, no comparison is possible between the density of molecules in the different phase-space diagrams. Only the structure of the phase-space distributions is of relevance here.

From Fig. 3 it is seen that for all values of ϕ_0, the separatrix accurately describes the longitudinal acceptance of the decelerator if the trajectories of the molecules are restricted to the molecular beam axis. The longitudinal phase-space distributions in the last stage of the decelerator are homogeneous, and no structure in the distribution is observed. The deviation of the phase-space distribution from the separatrix for $\phi_0>0°$ results from the relatively low velocity ($\sim$70 m/s) of the synchronous molecule in the last electric field stage of the decelerator. For these velocities, the Stark energy of the molecules in the field is not negligible compared to the kinetic energy and the assumptions that are used in the derivation of the model for phase stability are not valid anymore [14]. However, these deviations from the model are unrelated to the three-dimensional motion of the molecules through the decelerator and will not be further discussed here.

In contrast to the 1D simulations, the phase-space distributions that result from the three-dimensional trajectory simulations are highly structured and this structure differs depending on the phase angle ϕ_0. For $\phi_0=0°$ the longitudinal phase-space distribution shows regions that are alternately empty and filled. In the center of the separatrix, only a limited number of molecules can be found that are phase stable. This is counterintuitive, as this implies that molecules that have a position in phase space close to the synchronous molecule are actually not so well transported through the decelerator. Surrounding this empty center, a stable ring is found. Even farther away from the center, the stable ring suddenly changes into an empty ring, referred to as a halo. Hardly any molecules exist in the last stage of the decelerator that have a position in phase space that is within this halo. Particularly interesting is the sharp boundary between the stable ring and the halo. Close to and on the separatrix, a thin outer stable ring appears.

For higher values of ϕ_0, the structure in the phase-space distribution changes. The empty area in the center vanishes rapidly and is already almost absent for $\phi_0=20°$. A stable region in the center of the separatrix, followed by an empty halo and a stable ring close to the separatrix, is observed for the phase angles $\phi_0=20°$ and $\phi_0=40°$. For $\phi_0=60°$, the halo gains in stability, although the highest stability can still be

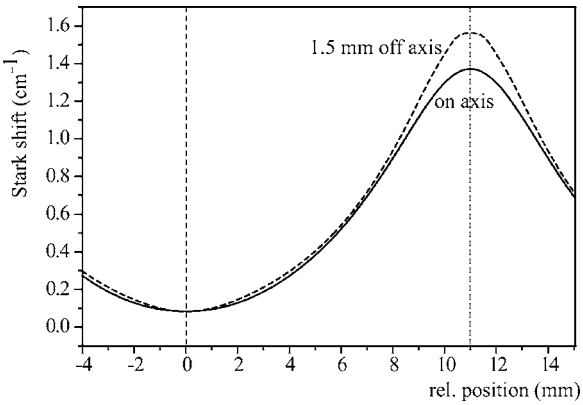

FIG. 4. Stark energy of an OH ($X^2\Pi_{3/2}$, $J=3/2$, $M_J\Omega=-9/4$) radical as a function of its longitudinal position in an electric field stage when the molecule flies on (solid curve) and 1.5 mm away from (dashed curve) the molecular beam axis. The positions of the electrodes are indicated by the vertical dashed lines.

found in the center of the separatrix. Although exhibiting a structured distribution, the extent of the phase-space distribution for phase angles up to 60° is well described by the separatrix. For $\phi_0=80°$, however, the majority of the molecules have a position in phase space that is outside the separatrix and the total area of the phase-space distribution largely exceeds the area of the separatrix.

The phase-space distributions of the molecules in the last stage of the decelerator for different values of ϕ_0, presented in Fig. 3, have important implications for the operation of a Stark decelerator. For low values of the phase angle ϕ_0, the acceptance of the decelerator is less than the model of phase stability suggests. Indeed, the simulations show that molecules with a position in phase space originally within the halo crash onto the electrodes somewhere during their path through the decelerator. For high values of ϕ_0, however, the acceptance of the Stark decelerator is actually significantly higher than can be expected from the model; a larger fraction of the molecular beam can be selected than indicated by the separatrix. Apart from these implications, the observed structure in the phase-space distributions, and in particular the structure for $\phi_0=0°$, indicates that interesting (and complex) six-dimensional phase-space dynamics of molecules in a Stark decelerator is present. In the following sections, the structure of the observed phase-space distribution for different values of ϕ_0 is explained in terms of a coupling between the transverse and longitudinal motion of the molecules in the decelerator.

C. Effective phase angle

The enhanced stability that occurs when the decelerator is operated at high phase angles can be understood from the potential energy of a molecule during its trajectory between two adjacent electric field stages. In Fig. 4 the Stark energy of an OH ($X^2\Pi_{3/2}$, $J=3/2$, $M_J\Omega=-9/4$) radical is shown as a function of its position in an electric field stage for two different trajectories of the molecule. The electrode positions are indicated by the vertical dashed lines. The electrodes at the positions 0 mm and 11 mm are grounded and placed at high voltage, respectively. In the dashed curve of Fig. 4, the Stark energy is shown when the trajectory of the molecule is parallel to, but 1.5 mm away from, the molecular beam axis. In the solid curve, the molecule is assumed, like in the one-dimensional model for phase stability, to fly along the beam axis. Clearly, for longitudinal positions close to the position of the electrodes that are placed at high voltage, the Stark energy of a molecule that has an off-axis position deviates significantly from the Stark energy on the molecular beam axis. This is expected, as the electric field close to the surface of the electrodes is higher than the electric field on the molecular beam axis. However, the time sequence for a given phase angle ϕ_0 that is applied to the decelerator is normally calculated for a synchronous molecule that flies along the molecular beam axis. The positions 5.5 mm and 11 mm in Fig. 4 correspond to the phase angles $\phi_0=0°$ and $\phi_0=90°$, respectively. However, Fig. 4 implies that the synchronous molecule actually observes the *lowest* difference in Stark energy during its trajectory between two successive switch times. For molecules that have off-axis velocity components, the time sequence that is applied actually matches with a time sequence that would have been obtained for a synchronous molecule with a lower value of ϕ_0. This situation is analogous to the discussion of the simultaneous deceleration of different ammonia isotopomers [14]. If a time sequence is generated for a molecule that can be least well decelerated, a molecule with a different Stark effect and/or different mass that is synchronous with this time sequence can be found as well. The longitudinal acceptance of the decelerator is smallest, however, for the molecule that can be least well decelerated. In the situation discussed here this implies that, for a given time sequence, molecules that do not fly along the molecular beam axis observe a larger longitudinal acceptance of the decelerator. Since in a laboratory molecular beam a large distribution of off-axis positions and velocity components is present, the longitudinal acceptance of the decelerator at high phase angles is best described by an "effective phase angle" $\phi_{0,eff}$ instead of ϕ_0, with $\phi_{0,eff}<\phi_0$. In Sec. IV A experiments are described where phase-stable deceleration of a package of OH radicals is observed when the Stark decelerator is operated at a phase angle $\phi_0=90°$.

D. Transverse stability

The structure in the longitudinal phase-space distribution that is observed when the Stark decelerator is operated at low phase angles is more complex. A good understanding of the processes that lead to this structure can be obtained by studying the three-dimensional trajectories of molecules in a Stark decelerator when the decelerator is operated at a phase angle $\phi_0=0°$. For this value of ϕ_0, the contrast between stable and unstable regions is maximal.

The reason for the low number of molecules that are found in the central region of the phase-space distribution can be directly inferred from Fig. 2. In this region, the phase of a molecule oscillates around the synchronous molecule with only a limited amplitude. The transverse frequency in this region is then too low to restrict the transverse trajectory

to the 4×4 mm^2 transverse spatial area that is given by the surfaces of the electrodes. Only molecules that have small transverse velocity components do not crash onto the electrodes somewhere downstream from the entrance of the decelerator. Although being inherently stable, the transverse acceptance of the decelerator in this region is small. Nonsynchronous molecules that have an ever larger displacement from the synchronous molecule in longitudinal phase space experience a higher transverse force, and the transverse acceptance of the Stark decelerator increases. The number of molecules that do not crash on the electrodes rises rapidly, and the phase-space distribution becomes more filled. When the Stark decelerator is operated at higher values of ϕ_0, the synchronous molecule approaches closer the set of electrodes that are at high voltage when the fields are switched. Compared to $\phi_0=0°$, phase-stable molecules are in a region where the transverse oscillation frequency is higher. The molecules are therefore more efficiently focused, and the empty central region becomes smaller for increasing values of ϕ_0. In the phase-space distributions of Fig. 3 it is seen that for $\phi_0>20°$, the empty central region in the longitudinal phase-space distribution already vanishes.

Referring back to Fig. 3, the halo in the longitudinal phase-space distribution for $\phi_0=0°$ cannot be understood from the argumentation that is presented above. On the contrary, for molecules with an ever larger displacement from the synchronous molecule, the Stark decelerator is expected to have a larger transverse acceptance. Apparently, the appearance of the halo is the result of an unstable behavior of the trajectory of molecules. This strongly suggests that the coupling between the longitudinal and transverse motion can indeed result in a parametric amplification of the (transverse) motion. In the next section we present a model for the transverse motion of molecules in a Stark decelerator, based on the time dependence of the transverse force, that leads to a quantitative understanding of the presence and location of the halo.

E. Transverse equation of motion, $\phi_0=0°$

In the derivation of the transverse equation of motion that is presented in this section, we will again limit ourselves to $\phi_0=0°$. It is clear from Fig. 4 that, in particular for low and moderate phase angles, the potential energy of a molecule that flies on or off axis is almost identical. In the model for the transverse motion presented in this section, we will therefore assume that the longitudinal frequency $\omega_z/2\pi$ does not depend on the transverse position of the molecule. The transverse oscillation frequency $\omega_y/2\pi$ as a function of time for a nonsynchronous molecule with a given initial longitudinal position z_i can then be calculated as is illustrated in Fig. 5. Let us consider a molecule with a certain initial longitudinal position z_i and some initial transverse position. The transverse oscillation frequency $\omega_y/2\pi$ as a function of the phase ϕ of this molecule, as already presented in Fig. 2, is shown on the right top corner of Fig. 5. The phase $\phi(t)$ oscillates with the longitudinal frequency $\omega_z/2\pi$ and is shown in the left top corner of Fig. 5. The value of $\omega_z/2\pi$ follows from the value of z_i (see Fig. 1). The outer turning points of the

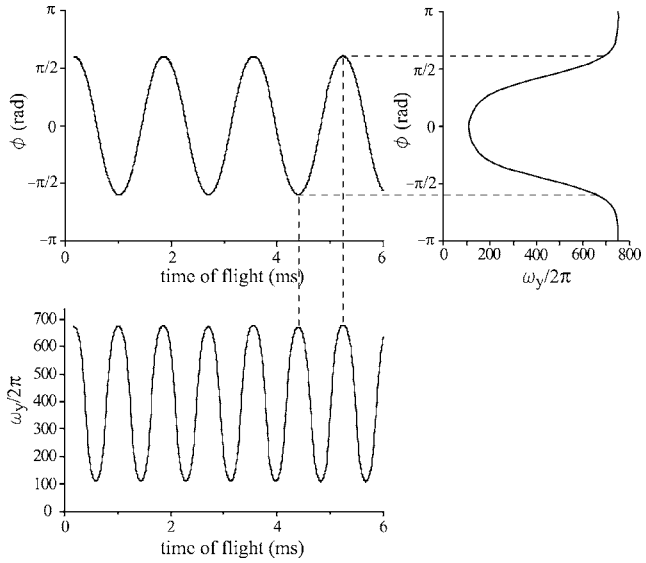

FIG. 5. The temporal dependence of the transverse oscillation frequency ω_y can be constructed from the temporal dependence of the phase ϕ in combination with the dependence of ω_y on ϕ (Fig. 2).

motion of the molecule are indicated by the horizontal dashed lines in Fig. 5. The temporal dependence of the transverse oscillation frequency $\omega_y(t)/2\pi$ can now easily be constructed and is shown in the lower curve of Fig. 5. It is readily seen that $\omega_y(t)$ oscillates with twice the longitudinal oscillation frequency. The transverse trajectory of the molecule can be calculated by solving the equation of motion

$$\frac{d^2y}{dt^2}+\omega_y^2(t)y=0. \tag{3}$$

To a good approximation, $\omega_y^2(t)$ can be represented as an oscillatory function:

$$\omega_y^2(t)=\omega_0^2-A\cos(2\omega_z t). \tag{4}$$

The transverse motion is driven by the longitudinal motion, and the transverse equation of motion is given by the well-known Mathieu equation [23]

$$\frac{d^2y}{d\tau^2}+[a-2q\cos(2\tau)]y=0, \tag{5}$$

with

$$a=\left(\frac{\omega_0}{\omega_z}\right)^2,\quad q=\frac{A}{2\omega_z^2},\quad \tau=\omega_z t. \tag{6}$$

Depending on the values of a and q, the solutions of the Mathieu equation exhibit stable or unstable behavior. This is shown in the Mathieu stability diagram in the left top corner of Fig. 6. The regions where stable solutions exist are indicated as gray areas; in the white regions, the solutions are exponentially unstable. For the equation of motion (5), $a\geqslant0$ and the largest unstable region appears around $a=1$. For this value $\omega_0=\omega_z$; i.e., the time-integrated transverse frequency $\omega_y/2\pi$ is equal to the longitudinal oscillation frequency $\omega_z/2\pi$, leading to parametric amplification of the

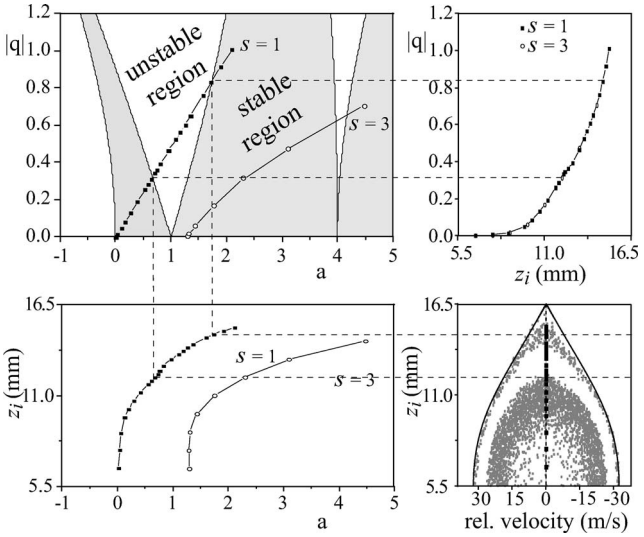

FIG. 6. Mathieu stability diagram, indicating whether the solutions of the transverse equation of motion are stable or unstable. The position in the stability diagram of a nonsynchronous molecule as a function of the initial longitudinal position z_i is indicated by the solid squares (open circles) if the Stark decelerator is operated at phase angle $\phi_0=0°$ using the resonance with $s=1$ ($s=3$). The longitudinal phase-space distribution of molecules that results from three-dimensional trajectory calculations is given for $s=1$ in the right bottom corner.

transverse trajectory. In general, instable regions appear as "tongues" that touch the a axis at $a=p^2$ ($p \in \mathbb{N}$) [24]. The value of q determines the width of the unstable region. The description of the transverse motion of molecules in a Stark decelerator as presented here is very similar to the description of ions that are stored in a Paul trap [25,26] or of ions that pass through a quadrupole mass spectrometer [27].

For different values of z_i, indicated by the solid squares in the phase-space distribution in the right bottom corner of Fig. 6, the values of ω_z, ω_0, and A, and hence the parameters a and q, can be determined following the methodology as outlined in Fig. 5. The resulting values of a and q as a function of z_i are indicated in the left bottom corner and the right top corner of Fig. 6, respectively. The corresponding locations in the Mathieu stability diagram are indicated as well. For molecules with an initial longitudinal position z_i that is close to the synchronous molecule, a and q are small and the Mathieu equation has stable solutions. For values of z_i that are further away from the synchronous molecule, however, both a and q significantly increase. Above a critical value, the trajectories suddenly become unstable. The value of z_i at which this resonance occurs is in quantitative agreement with the position of the appearance of the halo in the phase-space distribution of the 3D trajectory simulation of molecules in a Stark decelerator. For even larger values of z_i (closer to the separatrix), the values of a and q are within a stable region in the stability diagram again. This is also observed in the phase-space distribution. The corresponding threshold value, however, does not exactly match the point where the halo changes into a stable region. This is mainly because the longitudinal motion is not harmonic, and for large values of z_i, $\omega_y^2(t)$ cannot accurately be represented by

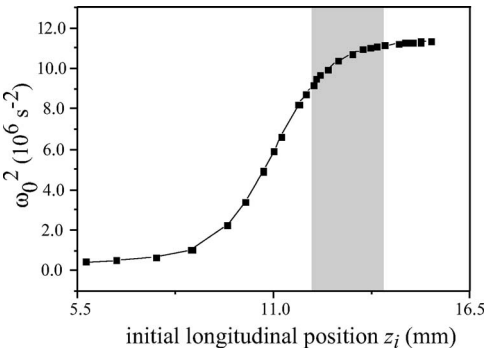

FIG. 7. The time-averaged transverse oscillation frequency ω_0^2 for an OH ($X^2\Pi_{3/2}$, $J=3/2$, $M\Omega=-9/4$) radical as a function of the initial longitudinal position in the Stark decelerator if the decelerator is operated at $\phi_0=0°$. The range in which the decelerator is unstable is indicated by the gray area.

Eq. (4). In these regions, a quantitative prediction from the model presented above cannot be expected.

The model for the transverse trajectory of molecules in a Stark decelerator presented above provides a clear understanding of the physical background for the presence of the halo. Molecules with a position in phase space within this halo experience a transverse force that is driven by the longitudinal motion in such a way that the transverse amplitude of the motion exponentially grows until the molecules crash onto the electrodes of the decelerator. This part of longitudinal phase space is therefore inherently unstable. Outside the halo, however, molecules within a certain transverse position and velocity interval—i.e., within the transverse acceptance of the Stark decelerator—will be bound within the 4×4 mm^2 spatial area that is given by the electrode array. The maximum transverse velocity component that is allowed for a molecule follows from the transverse force [Eq. (4)] that a molecule experiences during its flight through the decelerator. The time-averaged transverse force constant is given by $m\omega_0^2$, leading to a maximum transverse well depth of $\frac{1}{2}m\omega_0^2(2\text{ mm})^2$. The maximal transverse velocity $v_{\max}$ that can be captured can then be estimated via $\frac{1}{2}mv_{\max}^2 = \frac{1}{2}m\omega_0^2(2\text{ mm})^2$. The dependence of ω_0^2 on the initial longitudinal position z_i is shown in Fig. 7. The range of initial longitudinal positions z_i in which the decelerator is unstable is indicated by the gray area. For molecules with an initial longitudinal position z_i that is close to the synchronous molecule (position 5.5 mm in Fig. 7), the maximal transverse velocity is approximately 1 m/s. For initial positions z_i of 11 mm and 15 mm, the transverse velocity acceptance is approximately 5 m/s and 7 m/s, respectively.

Strictly speaking, the model described above is only valid when the Stark decelerator is operated at phase angle $\phi_0 = 0°$. Only then can $\omega_y^2(t)$, in a good approximation, be represented as a sinusoidally oscillating function, leading to the Mathieu equation for the transverse equation of motion. For higher values of ϕ_0, the function $\omega_y^2(t)$ is still periodic, but additional terms in the equation of motion (5) are needed to account for the nonsinusoidal character of ω_y^2. The equation of motion then transforms from the Mathieu equation into the less-well-known Hill [28] equation. Again, the solutions

of this equation exhibit stable and unstable behavior, although more parameters than just a and q determine the stability. A detailed analysis of the corresponding equations of motion is beyond the scope of this paper, but it is believed that a quantitative description of the halos that appear for the phase angles $\phi_0=20°$, 40°, and 60° in Fig. 3 can be obtained as well. For (much) higher values of ϕ_0, the y dependence of ω_z becomes important and will determine the acceptance of the Stark decelerator, as described in Sec. III C.

F. Higher-order resonances

So far, the transverse motion is analyzed in situations where the Stark decelerator is operated using the resonance with $s=1$—i.e., the situation where the synchronous molecule travels a distance L before the fields are switched. In this section the influence of the transverse motion of the molecules on the longitudinal acceptance of the decelerator is discussed if the decelerator is operated at $\phi_0=0°$ on a resonance with $s>1$. The strongest of these higher-order resonances is the resonance with $s=3$. The longitudinal motion of the molecules through the decelerator is fundamentally different if the decelerator is operated at a higher-order resonance. For instance, compared to normal ($s=1$) operation of the Stark decelerator, the synchronous molecule travels a distance that is equal to 3 instead of 1 electric field stage(s) before the fields are switched if the decelerator is operated at $s=3$ [20]. The synchronous molecule therefore always traverses a set of electrodes that is at high voltage during its path between successive switch times. The transverse focusing properties of the decelerator are therefore fundamentally different as well: the synchronous molecule is more strongly focused, and the transverse oscillation frequency of molecules that are close to the synchronous molecule will be higher.

In the left-hand side of Fig. 8, the longitudinal phase-space acceptance and the corresponding natural longitudinal and transverse oscillation frequencies are summarized, which are present when the decelerator is operated at $\phi_0=0°$ using the resonance with $s=1$. The initial longitudinal positions z_i that lead to the empty center or the halo are indicated by the gray areas. In the right-hand panel of Fig. 8, the longitudinal and transverse natural frequencies of the decelerator are shown for an OH ($X^2\Pi_{3/2}$, $J=3/2$, $M_J\Omega=-9/4$) radical if the Stark decelerator is operated at $\phi_0=0°$ using the first-order resonance with $s=3$. All other parameters are identical to the parameters used in the numerical simulations before. The transverse oscillation frequency for a molecule that is close to the synchronous molecule is indeed much larger compared to operation of the decelerator at $s=1$. In addition, the value of the natural transverse frequency depends less on the phase ϕ of the molecule. The natural longitudinal frequency is scaled down by a factor $\sqrt{3}$ compared to $s=1$, as predicted by the extended 1D model for phase stability [20]. During the motion of a molecule in the decelerator, the transverse natural frequency always exceeds the longitudinal natural frequency. Consequently, the coupling between the longitudinal and transverse motion will be profoundly different than if the Stark decelerator is operated at $s=1$. In the right upper corner

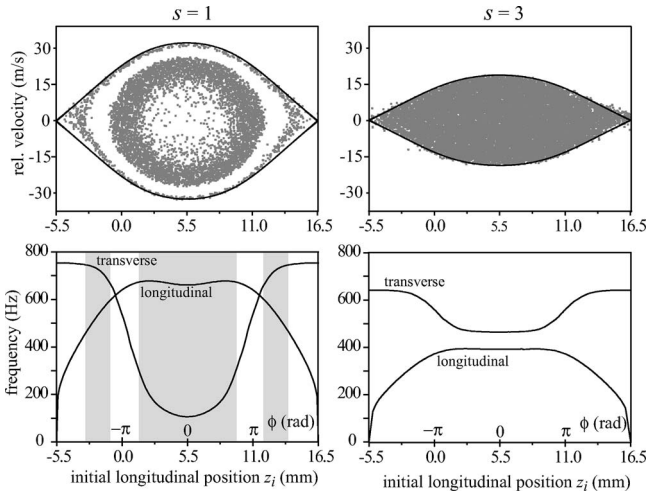

FIG. 8. Natural transverse and longitudinal oscillation frequency of an OH ($X^2\Pi_{3/2}$, $J=3/2$, $M_J\Omega=-9/4$) radical as a function of the initial longitudinal position z_i in the first electric field stage of the Stark decelerator. The decelerator is operated at $\phi_0=0°$ using the resonance $s=1$ (left-hand side) and $s=3$ (right-hand side). In the upper part the longitudinal phase-space acceptance of the Stark decelerator is shown for both cases. The initial longitudinal positions that lead to the empty center or the halo are indicated by the gray areas.

of Fig. 8, the longitudinal phase-space distribution of the molecules in the last stage of the decelerator is shown, which results from a three-dimensional trajectory simulation. The phase-space distribution is homogeneous, and no regions of instability or reduced acceptance are observed. The transverse acceptance at the center of the phase-space region is enhanced by the improved transverse focusing that is present in this region, and no empty center is observed. In addition, the halo is absent due to the (more) uncoupled longitudinal and transverse motion. Analogous to the methodology that was used in Sec. III E, the parameters a and q of the transverse equation of motion can be determined. These are shown by the open circles in the Mathieu stability diagram of Fig. 6 as a function of z_i. Indeed, when the Stark decelerator is operated using the resonance with $s=3$, the large unstable region centered around $a=1$ is avoided and the equation of motion has stable solutions. Only for large initial longitudinal positions does there exist a small unstable region centered around $a=4$. A region of reduced stability is indeed observed close to the separatrix in the numerical trajectory simulations, but a much larger number of stages in the decelerator is required before the molecules in this region are completely depleted.

Although the 1D model for phase stability predicts a phase-stable region that is scaled down by a factor $\sqrt{3}$ if the Stark decelerator is operated at the resonance $s=3$, the improved focusing properties of the decelerator, and the absence of the halo, actually result in a number of molecules that exit the decelerator that is more than a factor of 2 increased compared to "normal" operation of the decelerator. A significant increase of signal intensity has indeed been observed in the measurements described in Ref. [20] when the Stark decelerator was operated at $\phi_0=0°$ using the resonance with $s=3$ instead of $s=1$.

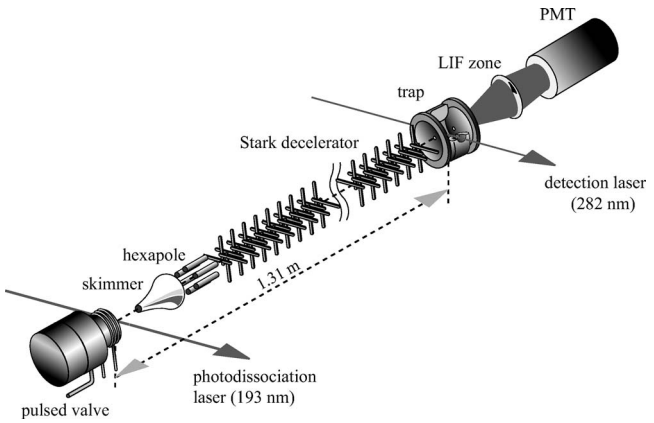

FIG. 9. Scheme of the experimental setup. A pulsed beam of OH radicals is produced via photodissociation of HNO_3 seeded in Xe. The beam passes through a skimmer, hexapole, and Stark decelerator and is detected via state-selective LIF detection inside the quadrupole trap. The trap is grounded in the present experiments.

IV. EXPERIMENT

It is very difficult to experimentally study the influence of the transverse motion of the molecules on the longitudinal phase stability in a Stark decelerator. Obviously, it is impossible to create a molecular beam in which all molecules exclusively fly along the molecular beam axis to make a comparison between the 1D and 3D cases. Nor is it possible to directly measure the longitudinal phase-space distribution of the molecules in the decelerator. At best, one can measure the spatial distribution of the molecular cloud in an electric field stage [29], but this does not yield the desired information on the phase-space distribution. The molecular beam deceleration machine used in this paper is best suited to record the time-of-flight (TOF) profile of the molecules that exit the decelerator. From the structure and the intensity of these TOF profiles, and from a comparison between the experimental profile and the profile that results from a 1D or a 3D trajectory simulation, a good insight into the phase-space distribution of the beam inside the decelerator can be obtained. This strategy is followed in the experiments reported here, in which the decelerator is operated in two limiting cases. In Sec. IV A experiments are described in which the decelerator is operated at a high value of ϕ_0 to verify the enhanced acceptance of the decelerator at these phase angles. In Sec. IV B the decelerator is operated at $\phi_0=0°$ to demonstrate the existence of the stable ring and the halo in the acceptance of the Stark decelerator.

The experiments are performed using the molecular beam deceleration machine that we employed recently for studying the existence of the higher-order resonances [20], as well as for the first experimental demonstration of the electrostatic trapping of OH radicals [8]. The molecular beam machine is schematically represented in Fig. 9. A pulsed beam of OH radicals is produced by photodissociation (193 nm) of HNO_3 molecules that are coexpanded with Xe from a pulsed solenoid valve, resulting in a molecular beam of OH radicals with a mean velocity around 365 m/s and with a velocity spread [full width at half maximum (FWHM)] of 15%. It is emphasized that when photodissociation is used for the generation of OH radicals, the beam is produced at a well-defined position and at a well-defined time. This greatly simplifies the interpretation of the observed TOF profiles of OH radicals exiting the decelerator. The hexapole, Stark decelerator, and electrostatic quadrupole trap have been discussed elsewhere [8,20]. The quadrupole trap is grounded in the present experiments. Inside the trap (1307 mm from the nozzle), the OH radicals are state-selectively detected using a laser-induced fluorescence (LIF) detection scheme. In our experiments, only the $M_J\Omega=-3/4$ and $M_J\Omega=-9/4$ components of the upper Λ-doublet state of the $J=3/2$ rotational ground state are focused by the decelerator and can contribute to the LIF signal.

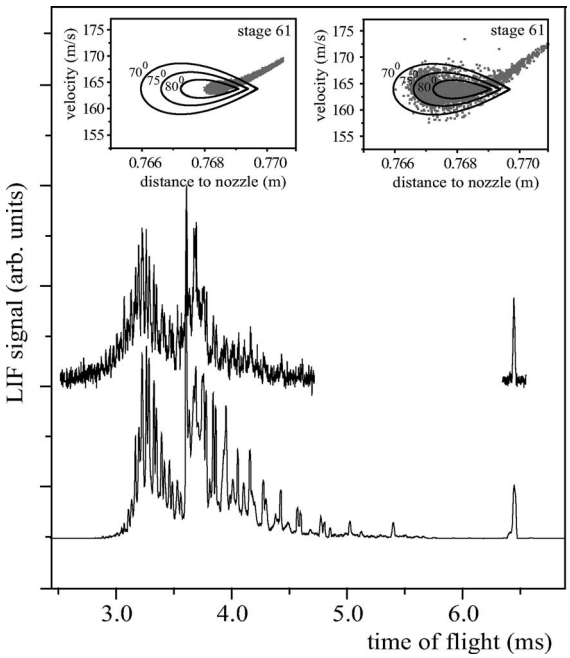

FIG. 10. Observed TOF profile of OH radicals that exit the decelerator when the decelerator is operated at a phase angle $\phi_0=90°$. The TOF profile that results from a three-dimensional trajectory simulation of the experiment is shown underneath the experimental profile. In the left and right insets, the longitudinal phase-space distribution of OH ($X^2\Pi_{3/2}$, $J=3/2$, $M_J\Omega=-9/4$) radicals in one of the last deceleration stages is shown, which result from a 1D and a 3D trajectory simulation, respectively. The separatrices that correspond to the phase angles $\phi_0=70°$, $\phi_0=75°$, and $\phi_0=80°$ are given as an overlay.

A. High phase angles: $\phi_0=90°$

To demonstrate the enhanced longitudinal acceptance of the decelerator for high values of ϕ_0, the decelerator can be operated with a time sequence that is calculated for a phase angle equal to 90°. In this case, phase stability vanishes in the one-dimensional model for phase stability; i.e., *only* the trajectory of the synchronous molecule is stable. In the upper curve of Fig. 10, the observed TOF profile is shown when the Stark decelerator is operated at a phase angle of $\phi_0=90°$ for a synchronous molecule with an initial velocity of 370 m/s.

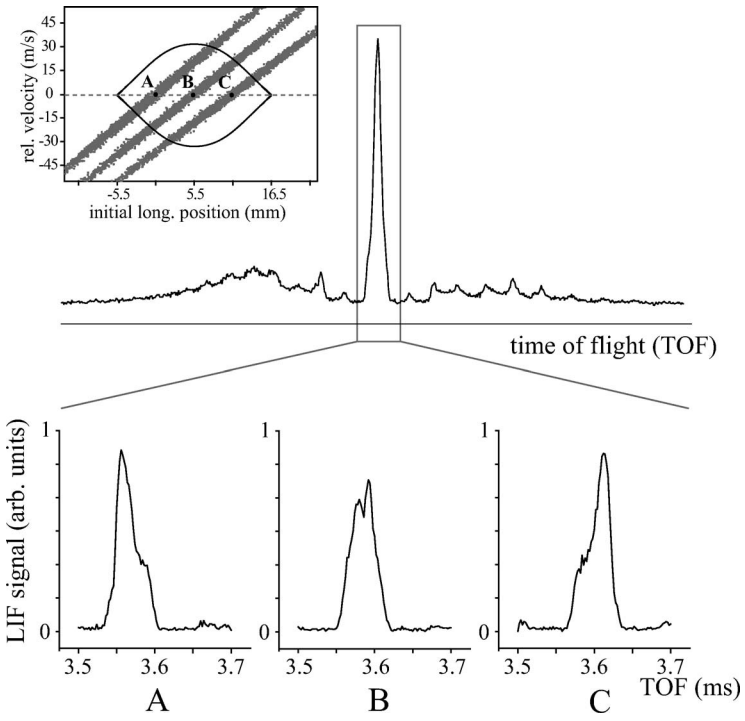

FIG. 11. Schematic representation of the experimental procedure to study the structure in the longitudinal phase-space acceptance when the Stark decelerator is operated at phase angle $\phi_0 = 0°$. In the upper part of the figure, the overlap of the acceptance of the Stark decelerator with the emittance of the molecular beam is shown for different initial longitudinal positions of the beam. For each of these initial positions, the TOF profile of molecules exiting the Stark decelerator is recorded and integrated in a 200-μs time window around the central peak.

With these settings of the decelerator, the synchronous molecule is decelerated to a velocity of 144.7 m/s in electric field stage number 65. The remaining stages are operated at $\phi_0 = 0°$ to transport the decelerated molecules to the detection region, where the synchronous molecule is expected to arrive about 6.4 ms after production. From the experimental profile it is clear that indeed a packet of molecules is captured by the decelerator and arrives in the detection region at the predicted arrival time. The observed TOF profile is accurately reproduced by the TOF profile that is obtained from a three-dimensional trajectory simulation of the experiment, shown underneath the experimental TOF profile. In the insets, the longitudinal phase-space distributions of OH ($X^2\Pi_{3/2}$, $J = 3/2$, $M_J\Omega = -9/4$) radicals in one of the last deceleration stages are shown, which result from a 1D (left inset) and 3D (right inset) trajectory simulation. The separatrices that correspond to $\phi_0 = 70°$, $\phi_0 = 75°$, and $\phi_0 = 80°$ are given as an overlay. The 1D trajectory simulation shows the presence of decelerated molecules if $\phi_0 = 90°$ is used, as our decelerator has a limited number of stages. These molecules, however, are not phase stable and spread out in phase space for increasing lengths of the decelerator. From the right inset it follows that when the decelerator is operated at $\phi_0 = 90°$, the decelerated molecules occupy an area in longitudinal phase space that is best described by an effective phase angle of 75°. This indicates that the transverse motion of the molecules through the decelerator results in an enhanced area of phase stability when the decelerator is operated at high phase angles.

B. Low phase angles: $\phi_0 = 0°$

When the Stark decelerator is operated at high phase angles like in the previous section, the longitudinal emittance of the molecular beam pulse largely exceeds the longitudinal acceptance of the Stark decelerator. The TOF profile of the decelerated molecules that exit the decelerator therefore directly reflects the (structure of) the phase-space distribution of the molecules in the last electric field stage of the decelerator. For low values of ϕ_0, however, the longitudinal acceptance of the decelerator can be much larger than the emittance of the beam. In particular, for the Stark decelerator and OH molecular beam used in this paper, the beam overlaps completely with the velocity interval of the longitudinal acceptance, but has a relatively narrow spatial distribution, which is predominantly determined by the spatial extent of the dissociation laser. If the molecular beam pulse (partially) overlaps with regions in longitudinal phase space that are unstable, the intensity of the TOF profile of the molecules that exit the decelerator will be reduced. By measuring the time-integrated intensity of the TOF profile at the exit of the decelerator as a function of the initial longitudinal position of the beam in the first electric stage, the overlap of the emittance of the beam with the longitudinal acceptance of the decelerator is probed. This strategy is used in the experiments that are described in this section. The experimental procedure is schematically represented in Fig. 11. In the inset in the upper left part of this figure, the longitudinal acceptance of the decelerator is shown if the decelerator is operated at phase angle $\phi_0 = 0°$. The initial position of the beam within this acceptance region can be selected by a proper choice of the time at which the decelerator is switched on with respect to the time that the OH radicals are produced. This is shown in the inset of Fig. 11 for three different initial longitudinal positions, referred to as *A*, *B*, and *C*. The longitudinal phase-space distribution of the beam is tilted as a result of the spreading of the beam between the nozzle and entrance of the Stark decelerator. The spatial extent of the dissociation laser in the experiments is reduced to 0.7 mm. As a result, the molecular beam only overlaps with the ac-

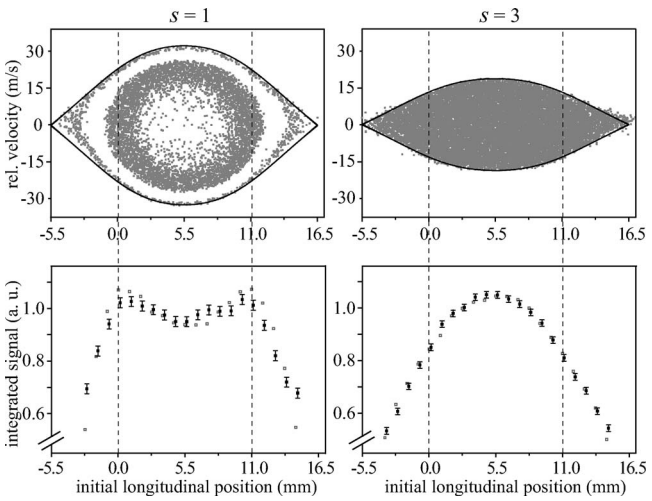

FIG. 12. Integrated signal intensity of a selected part of the TOF profile as a function of the initial longitudinal position of the beam, which is obtained when the Stark decelerator is operated at $\phi_0 = 0°$ using the resonance $s=1$ (left-hand side) and the resonance $s=3$ (right-hand side). The integrated signal intensities that result from a three-dimensional trajectory calculation of the experiment are indicated by the open gray squares. The longitudinal phase-space acceptance of the Stark decelerator for OH ($X^2\Pi_{3/2}$, $J=3/2$, $M_J\Omega=-9/4$) radicals is shown in the upper part for both cases. The positions of the electrodes of the Stark decelerator are indicated by the vertical dashed lines.

ceptance region in a spatially narrow and well-defined region. The integrated TOF profile of the molecules that exit the decelerator for a given initial longitudinal position of the beam therefore directly reflects the stability of that particular part of the phase-space acceptance region. By measuring the TOF profiles for various initial longitudinal positions of the beam, the structure within the longitudinal phase-space acceptance of the Stark decelerator can be probed. In the upper part of Fig. 11, a typical TOF profile is shown that is obtained if the decelerator is operated at phase angle $\phi_0=0°$. The central peak in this profile corresponds to phase-stable molecules—i.e., to those molecules that were within the longitudinal acceptance of the decelerator when the decelerator was switched on. For each initial longitudinal position of the beam, the TOF profile is recorded and integrated in a 200-μs time window around the mean arrival time of the central peak. This is indicated in the lower part of Fig. 11, where the TOF profiles are shown that are obtained when the beam is at the initial longitudinal positions *A*, *B*, and *C*.

On the left-hand side of Fig. 12, the integrated signal intensity of the experimentally obtained TOF profile is shown as a function of the initial longitudinal position of the beam in the Stark decelerator when the decelerator is operated at the phase angle $\phi_0=0°$ using the resonance $s=1$. For each longitudinal position of the beam, the TOF profile is recorded and integrated as discussed above. The resulting experimental data, together with the error bars, are represented by the solid squares in the lower panel of the figure. The longitudinal acceptance of the Stark decelerator for this case, already discussed before and shown in Fig. 8, is shown once more in the left upper panel of Fig. 12. The position of the electrodes is again indicated by the vertical dashed lines. It is noted that this phase-space distribution results from a simulation that is performed for a beam with a mean velocity of 250 m/s and a Stark decelerator that consists of 180 stages. In the experiments, however, the OH beam has a mean velocity of 365 m/s and the Stark decelerator that is used in the experiments consists of only 101 stages. This does not affect the inherent longitudinal acceptance of the Stark decelerator, but the relatively short amount of time that the molecules spend in the decelerator may result in a reduced contrast between the stable and unstable regions. Nevertheless, Fig. 12 shows that the molecules are most efficiently transported through the decelerator if the beam is coupled in at the longitudinal positions where the beam has most overlap with the stable ring in the phase-space acceptance. A clear decrease in signal is observed when the beam is initially in between these positions, at the center of the acceptance region. A sharp decrease in signal results when the beam has an initial position that is within the halo. The relatively small stable region that is close to the separatrix cannot be probed, as the TOF profiles that result when the beam is coupled in this region are difficult to interpret and cannot be accurately quantified. The dependence of the observed signal intensity on the initial longitudinal position of the beam in the first stage of the decelerator is a clear indication of the existence of both the small transverse acceptance at the center of the phase-space acceptance and of the halo. The integrated intensities of the selected intervals of the TOF profiles that result from a three-dimensional trajectory simulation of the experiment, taking both low-field seeking $M_J\Omega$ components of the $^2\Pi_{3/2}$, $J=3/2$ state of OH into account, are represented by the open gray squares in Fig. 12. Quantitative agreement between the observations and the simulations is obtained.

The experiments described above are repeated with the Stark decelerator operating at $\phi_0=0°$ using the resonance with $s=3$. The experimental results are shown in the right-hand side of Fig. 12. The homogeneous longitudinal phase-space acceptance that is present in this case results in a different dependence of the signal intensity on the initial longitudinal position of the beam. The largest fraction of the beam is selected and transported through the machine when the beam is coupled in at the center of the acceptance region, and this decreases further outward. The signal intensities that result from three-dimensional trajectory simulations are given as an overlay. Again, quantitative agreement is obtained between the observations and the simulations.

V. CONCLUSIONS

In this paper, the influence of the transverse motion on the longitudinal phase stability in a Stark decelerator is studied using OH radicals as a model system. For high values of the phase angle ϕ_0 ($\phi_0 > 70°$), the longitudinal phase-space acceptance of the decelerator is significantly enhanced by the transverse motion; a much larger part of the beam can be decelerated than the one-dimensional model for phase stability suggests. For low values of the phase angle ϕ_0, however, the transverse motion reduces the acceptance of the decelera-

tor; weak transverse focusing of the molecules results in a small transverse acceptance in the phase-space region around the synchronous molecule. In addition, coupling between the transverse and longitudinal motion can result in inherently unstable regions in phase space; driving of the transverse motion by the longitudinal motion can lead to unstable trajectories. A comprehensive model for the combined transverse and longitudinal phase stability, which provides a clear physical understanding of the presence of these effects, is presented.

The influence of the transverse motion on the longitudinal acceptance that is studied in this paper is generally present in Stark decelerators with the original design of the electrode array. The extent to which this results in a significant enhancement of the acceptance, or in an unacceptable reduction in efficiency of the decelerator, critically depends on a variety of parameters. Reduction of the longitudinal phase-space stability for low values of ϕ_0 will be more severe if molecules spend a longer time in the decelerator—i.e., for long Stark decelerators and/or for low velocities of the molecular beam. The structure of the phase-space distribution does not depend critically on the ratio of the (electric-field-dependent) Stark shift over mass of the molecule, however. The effects as discussed in this paper for the OH ($J=3/2$, $M_J\Omega=-9/4$) radical, with its (near) linear Stark effect, are generally present for molecules that exhibit a linear Stark effect. In particular, the halo is found at exactly the same position for OH radicals in the ($J=3/2$, $M_J\Omega=-3/4$) level, even though these experience a 3 times smaller Stark shift. This is readily understood as only the ratio of the transverse and longitudinal forces determines the unstable regions in phase space. But also for the molecules SO_2, H_2O, and H_2CO, which exhibit nonlinear Stark shifts, the phase-space distributions that result from three-dimensional trajectory simulations show a similar structure as the distributions that are obtained for OH. Only the overall longitudinal and transverse acceptance is different for the various molecules.

Stark decelerators are developed and built with the aim to decelerate (and ultimately trap) molecules. Apart from revealing complex and interesting six-dimensional phase-space dynamics of molecules in a Stark decelerator, the deviations from the acceptance that is predicted by the one-dimensional model for phase stability have profound consequences for the efficiency of the deceleration process. So far, in most of our trapping experiments, the phase angles that are used are equal to or exceed 70°, exploiting the increased acceptance of the decelerator that is present at these phase angles. An apparent obvious strategy to construct a Stark decelerator with a large number of stages, such that it can be operated at rather low phase angles [22], should be carefully considered; the increase in longitudinal phase-space acceptance that is present at lower phase angles might be undone by the inferior focusing properties of the decelerator and by the existence of inherently unstable regions. With the present design of the electrode geometry, a significant gain in the inherent longitudinal phase-space acceptance can only be obtained if the geometry and/or the applied electric fields are scaled up, although this is accompanied by severe technical difficulties [8]. When a decelerator with a design of the electrode geometry that allows for independent control over the transverse and longitudinal motion of the beam, as, for instance, applied in decelerators of the "alternating gradient" type [30], is used, a significant increase of the longitudinal phase-space acceptance of the decelerator can be obtained. This can also be achieved in the present design by operation of the decelerator using resonances with $s \geqslant 3$, although a larger number of electric field stages is required to obtain the same final velocity of the molecular beam. Whatever strategy is followed, detailed three-dimensional numerical trajectory simulations should be an integral part in the design of a new Stark decelerator apparatus.

ACKNOWLEDGMENTS

This work is part of the research program of the "Stichting voor Fundamenteel Onderzoek der Materie" (FOM), which is financially supported by the "Nederlandse Organisatie voor Wetenschappelijk Onderzoek" (NWO). This work is supported by the EU "Cold Molecules" network. We thank P.H.M. Smeets for his expert technical support and E. Hudson for fruitful discussions.

[1] H. L. Bethlem, G. Berden, and G. Meijer, Phys. Rev. Lett. **83**, 1558 (1999).
[2] J. R. Bochinski, E. R. Hudson, H. J. Lewandowski, G. Meijer, and J. Ye, Phys. Rev. Lett. **91**, 243001 (2003).
[3] M. R. Tarbutt, H. L. Bethlem, J. J. Hudson, V. L. Ryabov, B. E. Saner, G. Meijer, and E. A. Hinds, Phys. Rev. Lett. **92**, 173002 (2004).
[4] H. L. Bethlem and G. Meijer, Int. Rev. Phys. Chem. **22**, 73 (2003).
[5] Special issue: Ultracold Polar Molecules [Eur. Phys. J. D **31**, 149 (2004)].
[6] H. L. Bethlem *et al.*, Nature (London) **406**, 491 (2000).
[7] J. van Veldhoven, H. L. Bethlem, and G. Meijer, Phys. Rev. Lett. **94**, 083001 (2005).
[8] S. Y. T. van de Meerakker, P. H. M. Smeets, N. Vanhaecke, R. T. Jongma, and G. Meijer, Phys. Rev. Lett. **94**, 023004 (2005).
[9] F. M. H. Crompvoets, H. L. Bethlem, R. T. Jongma, and G. Meijer, Nature (London) **411**, 174 (2001).
[10] J. van Veldhoven *et al.*, Eur. Phys. J. D **31**, 337 (2004).
[11] S. Y. T. van de Meerakker, N. Vanhaecke, M. P. J. van der Loo, G. C. Groenenboom, and G. Meijer, Phys. Rev. Lett. **95**, 013003 (2005).
[12] S. Y. Lee, in *Accelerator Physics* (World Scientific, Singapore, 1999).
[13] H. L. Bethlem, G. Berden, A. J. A. van Roij, F. M. H. Crompvoets, and G. Meijer, Phys. Rev. Lett. **84**, 5744 (2000).
[14] H. L. Bethlem, F. M. H. Crompvoets, R. T. Jongma, S. Y. T. van de Meerakker, and G. Meijer, Phys. Rev. A **65**, 053416 (2002).
[15] G. Dong, W. Lu, and P. F. Barker, Phys. Rev. A **69**, 013409

(2004).
[16] R. Fulton, A. I. Bishop, and P. F. Barker, Phys. Rev. Lett. **93**, 243004 (2004).
[17] Y. Yamakita, S. R. Procter, A. L. Goodgame, and T. P. Softley, J. Chem. Phys. **121**, 1419 (2004).
[18] E. Vliegen, H. J. Wörner, T. P. Softley, and F. Merkt, Phys. Rev. Lett. **92**, 033005 (2004).
[19] N. Vanhaecke, D. Comparat, and P. Pillet, J. Phys. B **38**, 409 (2005).
[20] S. Y. T. van de Meerakker, N. Vanhaecke, H. L. Bethlem, and G. Meijer, Phys. Rev. A **71**, 053409 (2005).
[21] B. Friedrich, Eur. Phys. J. D **31**, 313 (2004).
[22] E. R. Hudson, J. R. Bochinski, H. J. Lewandowski, B. C. Sawyer, and J. Ye, Eur. Phys. J. D **31**, 351 (2004).
[23] L. D. Landau and E. M. Lifshitz, *Mechanics* (Pergamon, Oxford, 1960).
[24] *Handbook of Mathematical Functions*, 9th ed., edited by M. Abramowitz and I. A. Stegun (Dover, New York, 1970).
[25] R. Alheit, X. Z. Chu, M. Hoefer, M. Holzki, G. Werth, and R. Blumel, Phys. Rev. A **56**, 4023 (1997).
[26] M. A. N. Razvi, X. Z. Chu, R. Alheit, G. Werth, and R. Blümel, Phys. Rev. A **58**, R34 (1998).
[27] W. Paul and H. Steinwedel, Z. Naturforsch. A **8**, 448 (1953).
[28] D. Zwillinger, *Handbook of Differential Equations*, 3rd ed. (Academic Press, Boston, 1997).
[29] J. R. Bochinski, E. R. Hudson, H. J. Lewandowski, and J. Ye, Phys. Rev. A **70**, 043410 (2004).
[30] H. L. Bethlem, A. J. A. van Roij, R. T. Jongma, and G. Meijer, Phys. Rev. Lett. **88**, 133003 (2002).